Polymer 50 (2009) 627–635

Contents lists available at ScienceDirect

Polymer

journal homepage: www.elsevier.com/locate/polymer

Coupling effects of spinodal decomposition and crystallization on mechanical properties of polyolefin blends

Liang Yang [a,b], Yanhua Niu [a], Howard Wang [c], Zhigang Wang [a,*]

[a] CAS Key Laboratory of Engineering Plastics, Beijing National Laboratory for Molecular Sciences, Institute of Chemistry, Chinese Academy of Sciences, Beijing 100190, PR China
[b] Graduate School, Chinese Academy of Sciences, Beijing 100049, PR China
[c] Department of Mechanical Engineering, State University of New York at Binghamton, Binghamton, NY 13902, USA

ARTICLE INFO

Article history:
Received 13 October 2008
Accepted 22 November 2008
Available online 30 November 2008

Keywords:
Polyethylene blends
Liquid–liquid phase separation
Tensile properties

ABSTRACT

The influences of preferentially occurred liquid–liquid phase separation (LLPS) and following crystallization processes on the mechanical properties of statistical copolymer blends of poly(ethylene-*co*-hexene) (PEH) and poly(ethylene-*co*-butene) (PEB) have been investigated in detail through tensile deformation tests with a relatively high extension rate to avoid the effect of interfacial properties of the blends. Crystallinity and lamellar thickness of the samples are estimated by using the wide-angle X-ray diffraction and small-angle X-ray scattering techniques, respectively. The tensile modulus and yield stress are found to increase with LLPS time up to 6 h, but decrease afterwards, under the conditions of temperature of 120 °C and isothermal crystallization time of 10 min. It is considered that the instantaneous tensile properties are substantially largely affected by the much perfect lamellar structures formed during crystallization with a long time prior LLPS step. This finding is further experimentally substantiated by the scanning electron microscope observation. Whereas the strain-hardening modulus described by a simple neo-Hookean relation increases with LLPS time and reaches a plateau after 6 h, which can be accounted for by the cooperation effect between amorphous entanglement density, insensitive to LLPS time, and crystallinity redistribution. The similarity of the results observed on the blends experiencing the spinodal decomposition (SD) process supports that the redistribution of crystallizable components contributes to the tensile stress increase, which is primarily controlled by the development of LLPS process. This simple relationship gives us a new insight of what controls the mechanical properties of the phase separated polymer blends and of how we might be able to predict the mechanical properties of as yet unmixed polymer pairs.

1. Introduction

Polyolefins industry based on olefin chemistry is receiving a lot of attention in plastic industry today, and its importance is increasing due to the low cost of manufacture and the enhanced product properties through the new catalyst developing and alloying processes. From both the fundamental and the application concerns, it is particularly important to understand how the mechanical properties of polyolefins, for example, the typical stress–strain curves and the key tensile properties, depend on the microstructures and the related morphological parameters. It has been reported that at low strains, the tensile modulus as well as yield stress of polyethylene depend not only on the crystallinity but also on the lamellar thickness [1]. Under the condition of high strain deformation, the characteristic parameters, e.g., the elongation strain at break and strain-hardening modulus, are usually discussed in terms of the molecular network, represented by the trapped chain entanglements in the amorphous phase and the crystallites acting as physical cross-links [2–5]. The increasing strain-hardening modulus as a function of crystallinity determined by neo-Hookean model is rationalized by an effective contribution of the chains anchored in adjacent crystallites to the network density [4]. However, the crystallinity is not the only concerned parameter, because the molecular structures including molecular weight and branching density also influence the strain-hardening behavior. Studies on linear polyethylene and random copolymers of ethylene indeed indicate a less strenuous relation between the entanglement densities, influenced by molecular weight, branch type and branch content, and the strain-hardening modulus [6,7].

Blending as an effective strategy to optimize the properties and processability of the final product of olefin polymers also makes their property expectation more complicated and difficult

* Corresponding author. Tel./fax: +86 10 62558172.
E-mail address: zgwang@iccas.ac.cn (Z. Wang).

0032-3861/$ – see front matter © 2008 Elsevier Ltd. All rights reserved.
doi:10.1016/j.polymer.2008.11.033

compared with the single components, due to their intricate phase transition coupling and the related morphological evolutions. Thus the majority of the limited investigations on this issue only restrict in the theoretical and microscopic fields. In recent years, the competition between LLPS and crystallization for the nearly isorefractive blends of statistically random poly(ethylene-*co*-hexene) (PEH) and poly(ethylene-*co*-butene) (PEB) copolymers has been extensively investigated [8,9]. The experimental results support the proposed mechanism of "fluctuations-assisted crystallization" [10], where the spontaneous fluctuations of LLPS can overcome the crystal nucleation barrier and assist the crystallization process. It has been shown that in a simultaneously crystallized and phase-separated polymer blend, the morphological development exhibits a "crossover" feature [11] from the dominant crystal lamellar morphology to dominant liquid–liquid phase coarsening morphology. Competition between LLPS and crystallization, depending on the crystallization temperature above or below this crossover, can affect the structural and morphological developments during crystallization of the blends on lamellar scales [12]. Moreover, an asymmetric distribution of crystals caused by LLPS has been reported in *it*-PP/*it*-P1B blend system [13] from the microscopic viewpoint.

Although the interplay between LLPS and crystallization and the redistribution of crystals induced by LLPS for polymer blends have been understood to a large extent, the remaining question is how strong effects the readily formed intrinsic complicated structure can bring on the final macroscopic mechanical properties. Besides, a long-standing theory that an inferior mechanical property upon blending polymer pairs only ascribes to the poor stress transfer between the co-continuous phase domains with sharp interface [14,15] should be reconsidered with respect to the effect of the structures inside the phase domains. To the best of our knowledge, no well-defined influences of the internal structures of phase domains on the final mechanical properties of polymer blends have been reported in the literature so far. In the particular PEH/PEB blends, the distributions of crystal lamellae and the chain entanglement density in phase domains are expected to depend on the competition between LLPS and crystallization. Meanwhile, the crystalline morphology and phase boundary that result from the potential liquid–liquid phase separation process should be considered in the analysis of tensile test data. Nevertheless, for partially miscible blend systems, such as the PEH/PEB blends, the ambiguous interface between phase domains and the much slow phase domain relaxation may minimize the contribution of interfacial tension on the tensile properties. A relatively high strain rate of 0.01 s^{-1} is employed in this study, for which the influences of phase boundary disappear as demonstrated later and this method provides a good platform and an elaborate perspective for investigating the contributions from the inside of phase domains, e.g., distributions of crystal lamellae, to the final mechanical properties.

The present work mainly focuses on investigating the effects of LLPS on mechanical properties at lamellar scales and clarifying the relationship between the microstructures and mechanical properties. Distinguishable LLPS times concomitant with different crystallization temperatures above and below the aforementioned crossover temperature were chosen to prepare the samples. Particular attention is paid to the samples, which crystallize at 120 °C for 10 min, where a remarkable coupling effect of LLPS and crystallization on the stress–strain curves exists. We will introduce and explain our experimental scheme, consider the changes of crystal lamellar distributions in our data analysis, and discuss the micromechanical background for the performance of mechanical properties. According to our knowledge, this is the first report about the novel rely of the mechanical properties on internal structures of phase domains for a polymer blend system.

2. Experimental section

2.1. Materials

The materials used in this study were supplied by ExxonMobil Co. Ltd. They were statistical copolymers of ethylene and 1-hexene (PEH, M_w of 110 kg/mol, with 2 mol% hexene comonomer) and of ethylene and 1-butene (PEB, M_w of 70 kg/mol, with 15 mol% butene comonomer). They were synthesized with metallocene catalysts and had relatively narrow polydispersity (~2). PEH was the only crystallizable component in the blend system throughout the experimental temperature conditions. Preparation of the blends followed the method described in a previous paper [9]. In this study, blends with 20%–90% mass fractions of PEH, denoted as H20–H90, respectively, were investigated.

2.2. Thermal treatments on the samples and mechanical tensile tests

The films of the blends with thickness of about 0.5 mm for the mechanical tensile tests were obtained by compression molding at 160 °C. The films were enclosed into an airproof aluminum box for thermal treatments in oil baths before the mechanical tensile tests. Two distinct thermal treatment processes were applied to the films.

As schematically shown in Fig. 1, the films in the aluminum box were firstly kept at 160 °C in the first oil bath for 10 min (denoted as t_h) to eliminate thermal history and were subsequently quenched to the designed phase separation temperature of 130 °C in the second oil bath for different time (denoted as $t_{ps} = 0$, 2, 6 and 20 h). Then, the films were quenched to the designed crystallization temperature T_c (100 or 120 °C) in the third oil bath for different time (denoted as $t_c = 5$ min or 10 h at 100 °C, and 10 min or 24 h at 120 °C). The temperature fluctuation during crystallization was less than ±0.1 °C. Finally, the films were quenched into liquid nitrogen. The treatment processes for all the blends were identical to ensure comparability and accuracy for the tensile tests.

The dog-bone shape specimens with length of 14.0 mm, width of 6.0 mm and width of 2.3 mm at the neck position were die-cut from the above films. Mechanical tensile tests with an 8 mm initial gage length and a strain rate of 0.01 s^{-1} were performed at room temperature by using an Instron Universal Testing Machine. Particular care was paid to the alignment of grips and specimen to

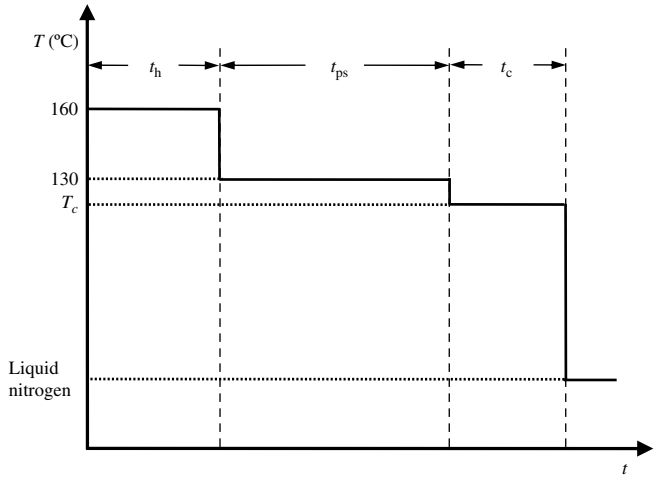

Fig. 1. Schematic illustration of the sample preparation processes. Annealing at 130 °C for different times and then isothermally crystallizing at 100 °C for 5 min or 10 h; or isothermally crystallizing at 120 °C for 10 min or 24 h. Here, t_h, t_{ps} and t_c denote melting time, LLPS time and isothermal crystallization time, respectively.

achieve uniaxial elongation. Tensile modulus was determined from the slope of the secant line at 0.5% strain because of the inconspicuous linear region on the stress–strain curve [16]. Yield stress was defined as the stress value at a point where the curvature of the stress–strain curve reached the maximum [17]. Tensile strength would not be used here because of the sample geometric limitation. The data reported for each film represented the averages of at least eight successful tensile tests. True stress could be derived from the following relation [17], assuming that the deformation was volume-invariant, where the localization phenomenon like necking was absent:

$$\sigma_{\mathrm{True}} = \lambda\sigma_{\mathrm{Eng}} = (1+\varepsilon_{\mathrm{Eng}})\sigma_{\mathrm{Eng}} \quad (1)$$

in which λ was the extension ratio.

2.3. Estimates of crystallinity and lamellar thickness

The values of crystallinity and lamellar thickness were obtained by using wide-angle X-ray diffraction (WAXD) and small-angle X-ray scattering (SAXS) techniques, respectively. Samples with thickness of about 0.5 mm were cut from the films, and were used to obtain 1-dimensional WAXD profiles and 2-dimensional SAXS patterns. The X-ray wavelength was 1.54 Å, and the sample-to-detector distance for the SAXS measurement was 1.5 m. The WAXD profiles in the diffraction angle range $2\theta = 5$–35° were collected on a Philips X'pert pro diffractometer with a 3 kW ceramic tube as the X-ray source (Cu Kα) and an X'elerator detector. Because of the broadened diffraction contribution from the amorphous phase, the crystallinity, X_c, was evaluated by a peak deconvolution procedure, which had been described elsewhere [18].

Lamellar thickness l_c could be generally determined from the z position at the peak in the interface distance distribution function which was identical with the second derivative of the 1-dimensional electron density correlation function, $K''(z)$ [19,20]. $K(z)$ could be calculated in a straightforward manner as Eq. (2) by Fourier transformation of the Lorentz-corrected SAXS intensity profile of $I(q)q^2$ versus q, where $I(q)$ was the scattering intensity [21].

$$K(z) = \frac{1}{2\pi^2}\int_0^\infty q^2 I(q)\cos(qz)\mathrm{d}q \quad (2)$$

This method for l_c estimation proved to be valid for the heterogeneous samples in our study, because the phase domains with micrometer sizes were much larger than crystalline lamellar stacks with nanometer sizes, thus, the characteristic peak on the scattering curve from the lamellar stacks would be free from the interference of phase domains.

2.4. Morphologies observed by using scanning electron microscopy

In order to observe the bulk morphologies, the films were fractured in liquid nitrogen. All fractured film surfaces were etched at room temperature for an appropriate time in 1% solution of potassium permanganate in a mixture of sulfuric acid and orthophosphoric acid, which preferentially etched the amorphous polymer in the crystals to make the crystal lamellae appear clearly. The fractured films were washed sequentially with hydrogen peroxide, distilled water and acetone, and then dried in a vacuum oven [22]. Before the SEM observation, the fractured film surfaces were coated with platinum.

3. Results and discussion

Fig. 2 shows the stress–strain curves of H50 with different LLPS times (0 h, 2 h, 6 h and 20 h) followed by crystallization at 120 °C for 10 min. For the samples crystallized at low crystallization temperature of 100 °C or high crystallization temperature of 120 °C with the long crystallization time of 24 h, the stress–strain curves are almost irrespective of the LLPS time, while for the samples crystallized at 120 °C for 10 min as shown in Fig. 2, the stress–strain curves are obviously affected by the LLPS time. The explanation to the former results is that the effects of LLPS may be covered by the relatively perfect crystallization processes with either high crystallization rate at low crystallization temperature or long crystallization time at high crystallization temperature. In the following sections, we pay our attention on the samples at the experimental conditions of crystallization temperature of 120 °C and crystallization time of 10 min and study the effects of interplay between LLPS and crystallization on the mechanical properties of the blends.

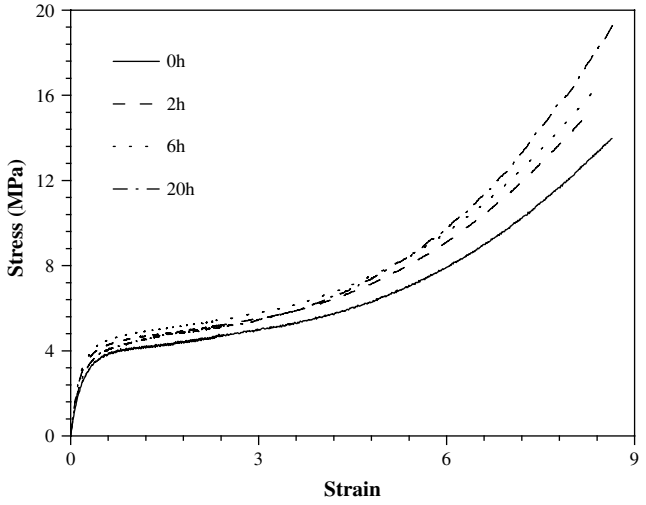

Fig. 2. Typical stress–strain curves for H50 with different LLPS times (0 h, 2 h, 6 h and 20 h) followed by crystallization at 120 °C for 10 min.

3.1. Low-strain tensile properties

The variations of low-strain tensile properties including tensile modulus and yield stress as functions of LLPS time for the different blends crystallized at 120 °C for 10 min are shown in Fig. 3. It can be seen from Fig. 3(a) that the tensile modulus of H50 in the 2 h and 6 h LLPS time cases increases about 16% compared with that with no LLPS, while the tensile modulus of H50 in the 20 h LLPS time case only increases slightly compared with that with no LLPS. Note the tensile modulus is determined from the slope of the secant line at 0.5% strain. The variations of tensile modulus of H40 and H60 as functions of LLPS time behave similarly because the spinodal decomposition (SD) process dominates at 130 °C for these three blends. On the other hand, for PEH, H90, H80 and H70 samples [23], the LLPS does not process through the SD mechanism; thus, the variations of tensile modulus of these blends with LLPS time do not show obvious changes within error limits. Similar trends for the variations of yield stress of the blends with LLPS time are evidently seen in Fig. 3(b).

It was previously reported that the instantaneous tensile properties of unoriented polyethylene were well known to vary linearly with crystallinity or density [24]. However, an unexpected result from our data is observed when we examine the dependences of low-strain tensile properties on the sample crystallinity. Although the values of crystallinity keep almost constant with LLPS time for H40, H50 and H60 as listed in Table 1, the tensile modulus and yield stress increase with LLPS time as shown in Fig. 3; thus, we consider that the variations of low-strain tensile properties may be more related to the crystalline lamellar thicknesses. As reported by Crist

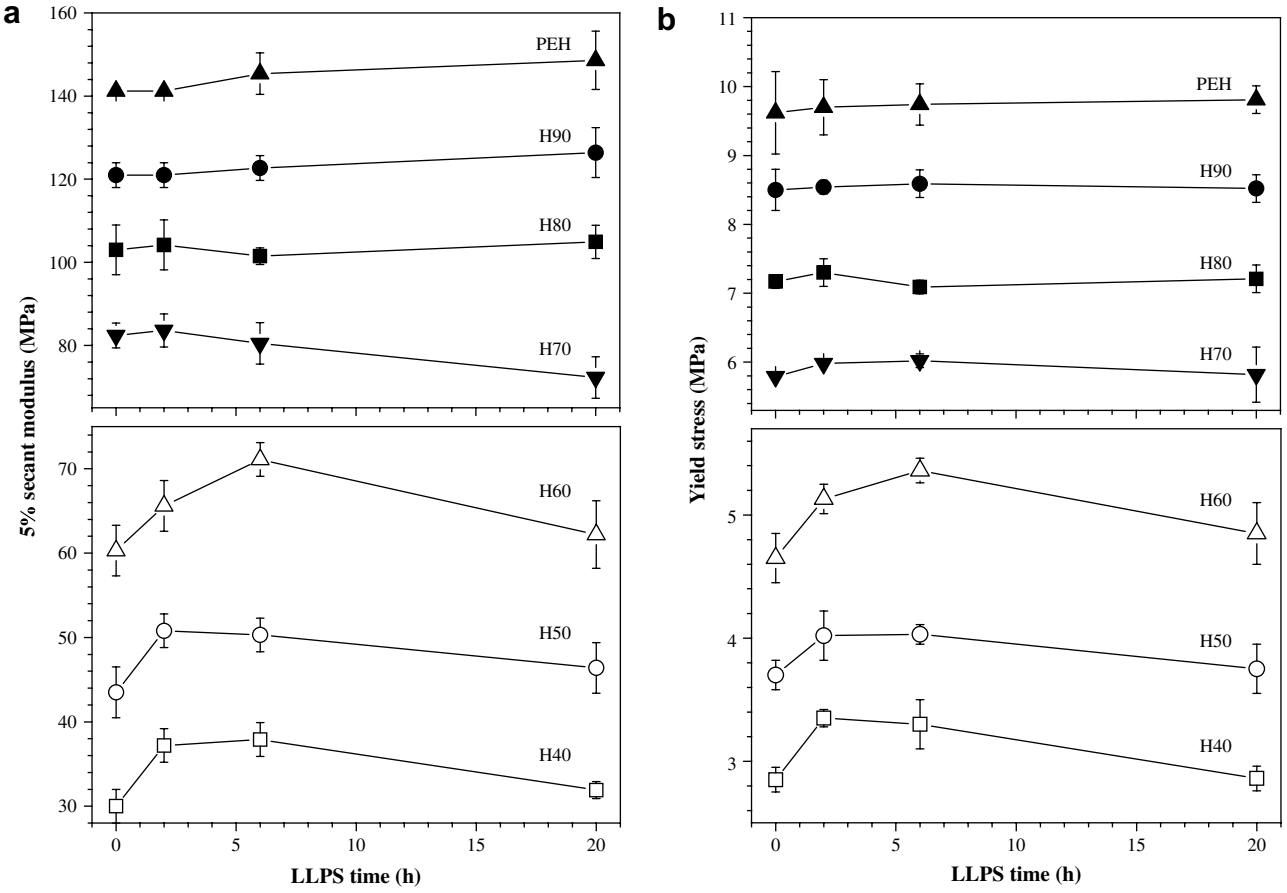

Fig. 3. Variations of (a) 5% secant modulus and (b) yield stress with different LLPS time for PEH/PEB blends with different compositions. The samples experienced LLPS at 130 °C and were followed by isothermal crystallization at 120 °C for 10 min.

et al., the prime determinant factor for the low-strain mechanical properties of polyethylene at room temperature is the crystalline lamellar thickness, l_c, which is related indirectly to crystallinity. Besides, the different curvature and segmentation inside the overall crystallite structure may also affect the yielding behavior [25]. To provide a possible explanation to our experimental results, we pay our attention to the differences in crystallite structure and morphology, particularly at crystalline lamellar scales. Fig. 4 shows the evolution of spinodal co-continuous morphologies of H50 at different LLPS time (the micrographs with amplified magnitude are put in the right panel). The increase in coarseness of the dispersed phase must be associated with an increase in the size of the PEB-rich domain that is extracted during the SEM sample preparation. It is observed that some short or granular crystals grow in the sample with no LLPS, and the crystal lamellae become longer and more perfect with prolonged LLPS time due to increasing crystallizable PEH concentration in the PEH-rich domains. Fig. 5(a) presents the Lorentz-corrected SAXS intensity profiles obtained for H50 with different LLPS times, and Fig. 5(b) presents the interface distance distribution functions derived from the SAXS intensity profiles. The first peaks shown in Fig. 5(b) relate to the crystallites: the location of the maximum yields the crystalline lamellar thickness, l_c (the standard deviation error $< 5\%$). Fig. 5(c) presents the variation of average crystalline lamellar thickness, l_c, as a function of LLPS time for H50. It is interesting to find that the increasing trend of crystalline lamellar thickness of H50 with LLPS time is basically consistent with that of the low-strain mechanical properties (from 0 h to 6 h case) as shown in Fig. 3. The obvious increase of crystalline lamellar thickness (roughly 21% from 0 h case to 2 h case) is largely ascribed to the fact that more crystallizable PEH component congregates in the PEH-rich domains with prolonged LLPS time.

The reliability of the obtained l_c values in the blends can be further confirmed by using a theoretical method, for which the most commonly used model that describes the dependence of true yield stress on crystalline lamellar thickness has been proposed by Young [26], Shadrake and Guiu [27]. The model assumes that yield involves thermal activation of screw dislocation with the Burgers vector parallel to the chain axis. According to the theory developed

Table 1
Values of crystallinity for PEH/PEB blends after different thermal treatment procedures. The samples experienced LLPS at 130 °C for different LLPS time and then were followed by isothermal crystallization at 120 °C for 10 min.

H20	H40				H50				H60				H70
	LLPS time (h)				LLPS time (h)				LLPS time (h)				
	0	2	6	20	0	2	6	20	0	2	6	20	
0.12	0.19	0.18	0.19	0.20	0.23	0.24	0.23	0.23	0.26	0.27	0.27	0.26	0.29

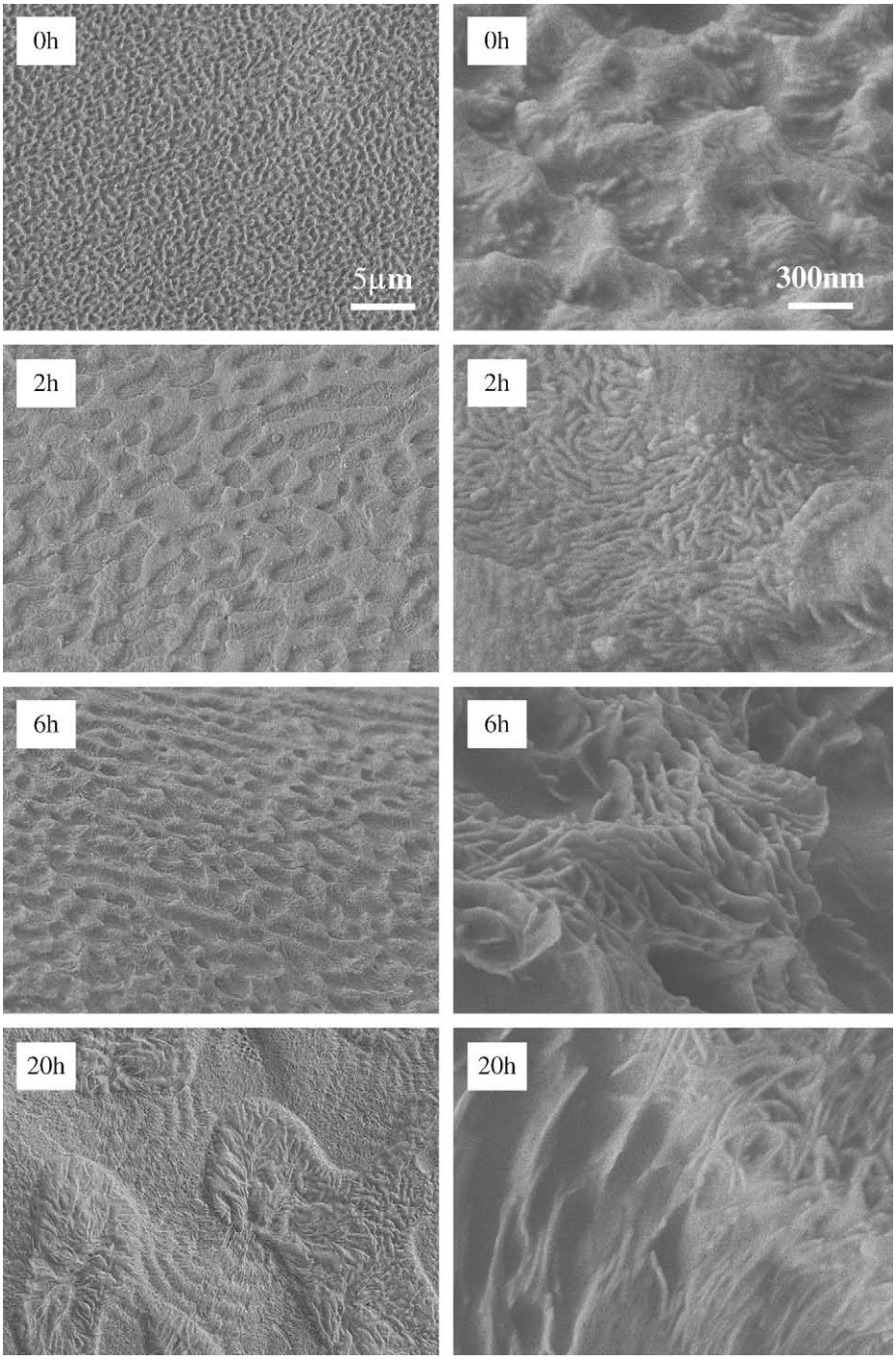

Fig. 4. SEM micrographs of H50 isothermally crystallized at 120 °C for 10 min after LLPS at 130 °C for different times (0 h, 2 h, 6 h and 20 h). The cryo-fractured cross-sections of the samples were observed. The scale bar in the left panel corresponds to 5 μm and that in the right panel corresponds to 300 nm.

and modified later by Brooks and Mukhtar [28], the true yield stress is given by [4]

$$\sigma_y = \frac{K}{\pi}\alpha(T)\exp\left(-\frac{2\pi\Delta G_c}{lKb^2}+1\right) \quad (3)$$

$$\alpha(T) = \frac{b}{r_0}\exp\left(\frac{2\pi E_0}{Klb^2}\right) \quad (4)$$

where ΔG_c relates to the change of the Gibbs free energy, with r_0 being the core radius of the dislocation, b the Burgers vector at distance d from the edge of the crystal, l the stem length (crystalline lamellar thickness), K a function of the crystalline shear modulus, and E_0 the core energy.

It is reported that ΔG_c is in the range of 40–60kT [27] with k the Boltzmann constant and T the absolute temperature. The value of K is taken from the theoretical work by Karasawa et al. [29]. Further, the value for the Burgers vector b is generally suggested to be 2.54 Å, and r_0 is assigned to equal 2b. By taking a value of ΔG_c of 60kT and $\alpha(T) = 1.481$ [28], $K = 2.359$ GPa [29] at 20 °C (= 293 K), the experimentally obtained and theoretically calculated true yield stresses as functions of LLPS time are compared in Fig. 6. The

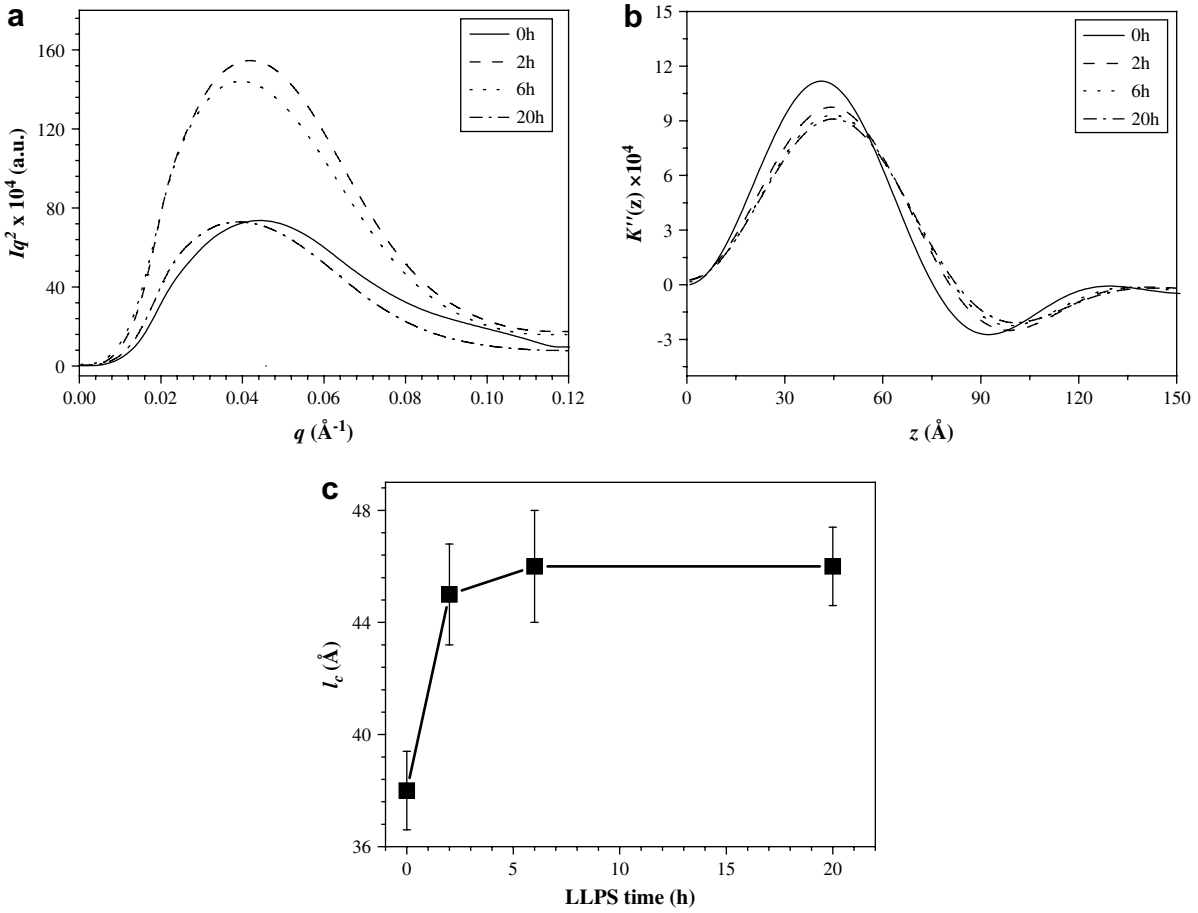

Fig. 5. (a) Lorentz-corrected SAXS intensity profiles of $I(q)q^2$ versus q; (b) interface distance distribution functions derived from the SAXS profiles shown in (a); and (c) variation of the average lamellar thickness with LLPS time for H50. The samples experienced LLPS at 130 °C and were followed by isothermal crystallization at 120 °C for 10 min.

qualitative agreement between the experimental and calculated results except the 20 h LLPS case proves the appropriate explanation of lamellar thickening mechanism to the increasing true yield stress.

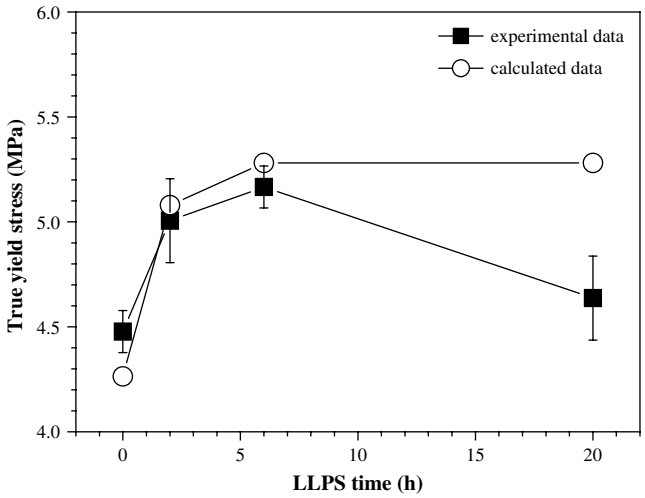

Fig. 6. Variations of the experimental (filled square) and theoretical (open circle) true yield stress of H50 with different LLPS time. The samples experienced LLPS at 130 °C and were followed by isothermal crystallization at 120 °C for 10 min.

Consequently, it would be instructive to consider how lamellae thicken in our case. Generally, isothermal thickening is a gradual process, with both thickening rate and final thickness increased by increasing crystallizable component concentration [30]. Similar results were reported by Cham et al. for *it*-PP/*it*-P_1B blends [13]. At high crystallization temperature, the melting point of crystals formed in the *it*-P_1B-rich phase was 8–10 °C lower than that in the *it*-PP-rich phase. On the contrary, at low crystallization temperature, the crystals formed in both phases melt approximately at the same temperature. In our case, at high crystallization temperature of 120 °C (>118 °C, the crossover temperature for H50 [11]), crystallization rate is relatively slow; thus, during crystallization SD simultaneously proceeds, which can assist crystallization as a driving force [10]. With increasing LLPS time and accordingly the well-developed phase domains, PEH concentration in the PEH-rich phase domains increases, which makes PEH crystallize more easily in the PEH-rich phase domains than the homogeneous melt with no LLPS, and the crystalline lamellar thickness is expected to increase as well. From the aforementioned mechanism, thicker lamellae can lead to higher tensile modulus for semicrystalline polymers, although the crystallinity does not show obvious changes. At the early deformation stage, polymer crystals deform plastically by crystallographic slip, when the resolved shear stress on the slip plane reaches a critical value, as known as the critical resolved shear stress [31]. Thicker lamellae in the PEH-rich phase domains with longer LLPS time require larger critical resolved shear stress, namely higher modulus and yield stress, to deform the sample when subjecting to an extension. Meanwhile, viscous

contribution from only the amorphous intercrystalline layers is considered as a minor part to modulus because interlamellar shear is an easier process with a lower energy consuming compared with intralamellar shear. Therefore, the changes of low-strain mechanical properties as shown in Fig. 3 reflect on some extent the dense assembly of crystallizable PEH component related to the LLPS process.

Interestingly, the low-strain tensile properties of H40, H50 and H60 apparently show slight depressions with more than 6 h LLPS time, and at the meanwhile, the calculated true yield stress of H50 is much higher than the experimental data (see Fig. 3). This experimental observation may reflect the contribution of phase structure besides the crystalline lamellar stacks. For example, the interphase volume decreases and the phase boundary sharpens (interphase shrinks) as the co-existent domains coarsen at the late stages of LLPS [10]. For the longest LLPS time (20 h), the enhancement of tensile modulus coming from lamellar thickening may be dramatically weakened by the largely sharpened phase boundary. Some other phase structures, such as the distribution of the phase domains and the shape of the phase domains may have to be assembled to account for this phenomenon as well. Further studies are necessary for providing a comprehensive understanding. In a word, all the summed contributions, e.g., those from crystalline lamellar thickness and phase structures, explain that an optimum of the low-strain tensile properties can be observed for the intermediate LLPS time case.

3.2. High-strain tensile properties

It is known that the amorphous regions in semicrystalline polymers such as polyethylene play a particular role for the large deformation behavior. Chain sequences in these regions have their ends more or less fixed, either by the existing chain entanglements or by being anchored in adjacent crystallites. This thus sets up a network, which can be stretched in a large deformation process. The strain-hardening at large deformation of H50 with different LLPS times has been shown in Fig. 2. We can observe that the upsweep of strain-hardening is much steeper and sets in at much lower nominal strain for the longer LLPS time case.

To learn more about the network properties, we follow a simple route devised by Haward and Thackray [32]. They have suggested that a partially crystallized polymer during deformation can be represented by the model shown in inset of Fig. 7. This model includes three parameters, low-strain tensile modulus, E, shear modulus of the network, G, and viscosity, η. Plot of σ versus $\lambda^2 - 1/\lambda$ yields two slopes, one starting from the origin, giving the Young's modulus, E, and the other one at high strains, giving the strain-hardening modulus, G, following a neo-Hookean description, which has been found to be valid for most polymers [33,34]. The changes of true stress with strain of $\lambda^2 - 1/\lambda$ for H50 are shown in Fig. 7, termed as the Haward–Thackray plots, in which the strain-hardening moduli are defined as the slopes at high strain ($\lambda = 2$), giving $G = 1.2$–1.4 MPa. Note that the strain-hardening moduli for polyethylene somewhat vary in literatures; however, they all fall in the range of 1–2 MPa [35].

Carrying out the Haward–Thackray plots for H40, H50 and H60 with different LLPS times and H20, H70 leads to the plots of strain-hardening modulus as functions of LLPS time shown in Fig. 8. One observes an increase in G with increasing crystallinity (from H20 to H70). The increase in G with increasing PEH content is, of course, conceivable, considering that the crystallites in the blends act in two ways to increase G, as fillers and anchors, which prevent crystal lamellar fragmentation [2]. Following this interpretation, a fact comes up: the strain-hardening modulus increases dramatically by about 16% from one case with no LLPS to the 20 h LLPS time case while the crystallinity remains invariant as known from Table 1 for each blend at a given content (H40, H50 and H60). This result although surprising at the first glance, is perfectly logical when considering the effects of spinodal decomposition (SD) for the cases of H40, H50 and H60. Note in Fig. 8 the G values for H20 and H70 (with no SD process) almost remain invariant for different LLPS times.

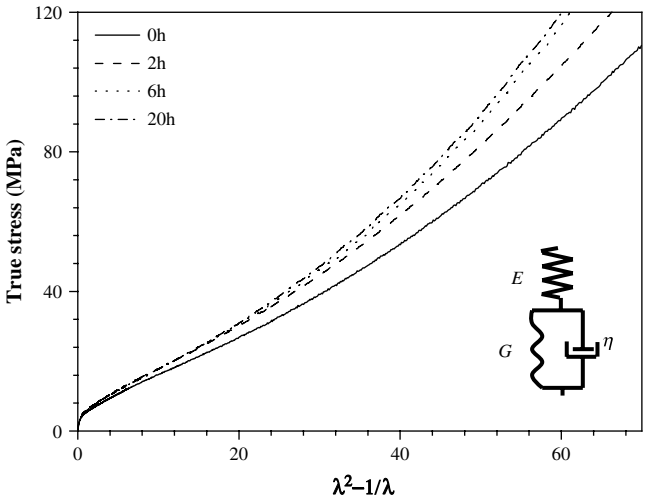

Fig. 7. Changes of true stress with strain of $\lambda^2 - 1/\lambda$ for H50 (the Haward–Thackray plot). The samples experienced LLPS at 130 °C and were followed by isothermal crystallization at 120 °C for 10 min.

Taking H50 as a typical example, and recalling the complicated intrinsic structures in the PEH/PEB blend, that is to say, an asymmetrical distribution of crystallinity naturally develops with high values in the PEH-rich domains and low values in the PEB-rich domains [9], it is reasonable to consider that H50 at the late stage (20 h) of LLPS at 130 °C separates into two phases with 20% and 70% PEH contents, respectively, according to the phase diagram [9]. Taking no account of the interfacial influence, H50 might be envisaged as a network including two entangled phases similar to H20 and H70, respectively, hypothetically the "H20" phase and "H70" phase [23]. Thus, the 20 h LLPS time case of H50 will be discussed in detail in the following section for a convenience purpose.

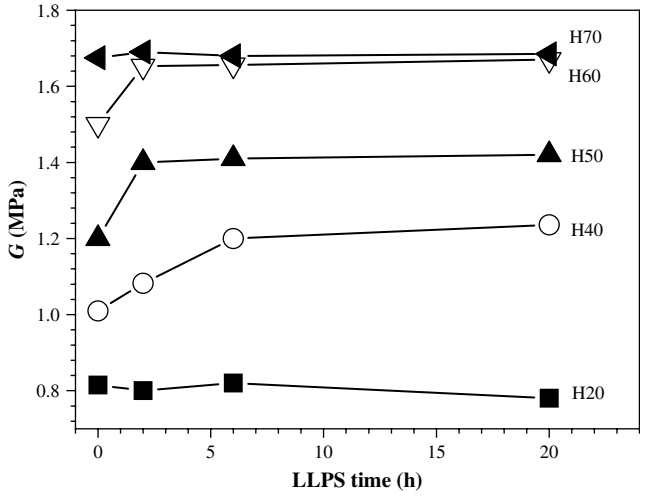

Fig. 8. Changes of strain-hardening modulus as functions of LLPS time for PEH/PEB blends.

As mentioned in Section 1, the strain-hardening behaviors are governed by the synergy of entanglement density in the amorphous region and viscous friction associated with the anchoring effect which is proportional to crystallinity in the crystalline phase. In particular, as well confirmed [3], the increase in strain-hardening modulus can be achieved normally by increasing the entanglement density or crystallinity. Obviously, a question is raised about which one is the main reason to cause the strain-hardening modulus increase in our case, either the entanglement density or the crystallinity which is related to the anchoring effect.

Molecular architecture dependence of the entanglement density in the amorphous phase for PEH/PEB blends should be considered at first as the molecular architecture, or even the entanglement density, may possibly change during the LLPS process. The plateau modulus can be transformed into network density by using the following Eqs. (5) and (6) [36,37] with assumption that the dynamics of polymer blends follows the description [38,39]:

$$G_N^0 = \frac{\rho_a RT}{M_e} \tag{5}$$

in which G_N^0 can be approximately estimated from the crossover modulus in the frequency sweep curves at 130 °C for H20, H50 and H70 [40], ρ_a is the polymer density in the molten state which should equal to the amorphous density of polyethylene ($\rho_a = 0.85$ g/cm^3) [4], R is the molar gas constant and T is the absolute temperature. The network density v_e can be calculated from M_e according to Eq (6):

$$v_e = \frac{\rho_a N_A}{M_e} \tag{6}$$

with N_A the Avogadro number. The yielded values of v_e for H20, H50 and H70 at 130 °C are 1.9×10^{26}, 2.0×10^{26} and 2.1×10^{26}, respectively, which evidently suggest that the entanglement densities are quite close to each other (the difference < 5%) in the molten state. For polymers, the existing entanglements cannot be resolved by crystallization from the quiescent melt, however, they shift into the amorphous regions [41]. It means that the isotropic entangled network in PEH/PEB melts at 130 °C will be retained in the amorphous phase after crystallization at 120 °C. Therefore, even though H50 totally phase-separates into the "H20" phase and "H70" phase with 20 h LLPS time, the approximately equal entanglement densities within the error limits cannot be mainly responsible for the difference of strain-hardening modulus between the 0 h and 20 h LLPS cases.

Since the possible molecular architecture effect has been excluded, the answer that the highly localized crystallinity accounts for the changes of strain-hardening modulus becomes more pertinent. The crystallinity and the strain-hardening modulus for H70 are both higher than that for H50 (see Table 1 and Fig. 8). Therefore, local anchoring effect of H50 for the 20 h LLPS time case caused by crystals is much higher than that for the 0 h LLPS time case due to the existence of "H70" phase with higher X_c. Higher crystallinity in the local "H70" phase domains in H50 with 20 h LLPS time elevates the strain-hardening modulus of H50 compared with the 0 h LLPS case. It can be deduced that the local "H70" phase domains in H50 with 20 h LLPS time increase the integral stress at high strains as a result of increased strain-hardening modulus, which means that the distribution of crystal structures holds the key to explain the effect of LLPS on the tensile properties. Although PEH concentration in each phase domain is difficult to experimentally determine for the 2 h or 6 h LLPS time case, the concentration fluctuations have almost reached equilibrium after 2 h LLPS time according to our rheological measurement [9]; thus, it is reasonable to speculate that the results for the 2 h and 6 h LLPS time cases, which are quite similar to the 20 h LLPS time case, can be explained also by the above reason. Moreover, the statement about crystal redistribution is valid for H40 and H60 too, which experience a similar LLPS process as H50. The novel relation between the strain-hardening modulus and crystallinity for H40, H50 and H60 can be well understood now.

4. Conclusions

The coupling effects of crystallization and spinodal decomposition on the tensile properties of the PEH/PEB blends in both low and high strain ranges have been investigated. By intentionally controlling the prior LLPS and subsequent crystallization conditions, tensile properties including both the yield stress and the accumulation of stress during the post yield deformation can be enhanced on some extent through prolonged LLPS time for H40, H50 and H60. At high extension rate, it is the crystal redistribution rather than interfacial tension that contributes to the tensile property enhancement. The low-strain properties, e.g., the tensile modulus and yield stress, increase sharply by 16% with increasing LLPS time from 0 h to 2 h and even to 6 h. It is considered that the much easier lamellar thickening within the PEH-rich phase domains with prolonged LLPS time rather than the increased crystallinity attributes to the above result. At high strains, the marked increase in strain-hardening modulus with prolonged LLPS time can be interpreted by the increasing local crystallinity without much change of the entanglement density. Although the averaged parameters, like crystallinity or entanglement density, do not change in the global range of the sample, the local assembly of more crystallizable PEH component is prone to enhance the critical stress to deform the sample in both the low and the high strain ranges. Controlling the liquid–liquid phase separation process is demonstrated as a novel and facile means for improving the physical properties of polymer blend materials.

Acknowledgments

The authors acknowledge the financial support from National Science Foundation of China with Grant Nos. 20674092 and 50573088 and National Science Foundation of China with Grant No. 10590355 for the State Key Project on Evolution of Structure and Morphology during Polymer Processing. HW acknowledges the support by the National Science Foundation of USA under Grant DMR-0711013. The authors would like to thank Prof. Erqiang Chen for the availability of the X-ray diffraction facility at the Peking University.

References

[1] Crist B, Fisher CJ, Howard PR. Macromolecules 1989;22:1709.
[2] Hiss R, Hobeika S, Lynn C, Strobl G. Macromolecules 1999;32:4390.
[3] Na B, Lv R, Xu W, Yu P, Wang K, Fu Q. J Phys Chem B 2007;111:13206.
[4] Schrauwen BAG, Janssen RPM, Govaert LE, Meijer HEH. Macromolecules 2004;37:6069.
[5] Takayanagi M, Nitta K. Macromol Theor Simul 1997;6:181.
[6] Kennedy MA, Peacock AJ, Failla MD, Lucas JC, Mandelkern L. Macromolecules 1995;28:1407.
[7] Kennedy MA, Peacock AJ, Mandelkern L. Macromolecules 1994;27:52970.
[8] Wang H, Shimizu K, Hobbie EK, Wang ZG, Meredith JC, Karim A, et al. Macromolecules 2002;35:1072.
[9] Niu YH, Wang ZG. Macromolecules 2006;39:4175.
[10] Zhang XH, Wang ZG, Muthukumar M, Han CC. Macromol Rapid Commun 2005;26:1285.
[11] Wang H, Shimizu K, Kim H, Hobbie EK, Wang ZG, Han CC. J Chem Phys 2002;116:7311.
[12] Wang ZG, Wang H, Shimizu K, Dong JY, Hsiao BS, Han CC. Polymer 2005;46:2675.
[13] Cham PM, Lee TH, Marand H. Macromolecules 1994;27:4263.
[14] Finlay J, Hill MJ, Barham PJ, Byrne K, Woogara A. J Polym Sci Part B Polym Phys 2003;41:1384.
[15] Pang YY, Dong X, Zhao Y, Han CC, Wang DJ. Polymer 2007;48:6395.

[16] Wang HP, Khariwala DU, Cheung W, Chum SP, Hiltner A, Baer E. Macromolecules 2007;40:2852.
[17] Sirotkin RO, Brooks NW. Polymer 2001;42:3791.
[18] Wang ZG, Hsiao BS, Sirota EB, Agarwal P, Srinivas S. Macromolecules 2000;33:978.
[19] Flores A, Pieruccini M, Nochel U, Stribeck N, Calleja FJB. Polymer 2008;49:965.
[20] Stribeck N, Alamo RG, Mandelkern L, Zachmann HG. Macromolecules 1995; 28:5029.
[21] Men Y, Strobl G. Macromolecules 2003;36:1889.
[22] Saengsuwan S, Bualek-Limcharoen S, Mitchell GR, Olley RH. Polymer 2003; 44:3407.
[23] Shimizu K, Wang H, Wang ZG, Matsuba G, Kim H, Han CC. Polymer 2004;45:7061.
[24] Peacock AJ, Mandelkern L. J Polym Sci Part B Polym Phys 1990;28:1917.
[25] Graham JT, Alamo RG, Mandelkern L. J Polym Sci Part B Polym Phys 1997;35:213.
[26] Young RJ. Philos Mag 1974;30:85.
[27] Shadrake LG, Guiu F. Philos Mag 1976;34:565.
[28] Brooks NWJ, Mukhtar M. Polymer 2000;41:1475.
[29] Karasawa N, Dasgupta S, Goddard WA. J Phys Chem 1991;95:2260.
[30] Hashida T, Jeong YG, Hua Y, Hsu SL, Paul CW. Macromolecules 2005; 38:2876.
[31] Galeski A. Prog Polym Sci 2003;28:1643.
[32] Haward RN, Thackray G. Proc R Soc London A Math Phys Sci 1968;302:453.
[33] Haward RN. Macromolecules 1993;26:5860.
[34] Haward RN. Polymer 1994;35:3858.
[35] Krigas TM, Carella JM, Struglinski MJ, Crist B, Graessley WW, Schilling FC. J Polym Sci Polym Phys Ed 1985;23:509.
[36] Liu CY, He JS, van Ruymbeke E, Keunings R, Bailly C. Polymer 2006;47:4461.
[37] van Melick HGH, Govaert LE, Meijer HEH. Polymer 2003;44:2493.
[38] Lorens J, Rude E, Marcos RM. Polymer 2003;44:1741.
[39] Wu J, Haddad TS, Kim GM, Mather PT. Macromolecules 2007;40:544.
[40] Niu YH. Ph.D. Dissertation, Institute of Chemistry, Chinese Academy of Sciences; 2006.
[41] Flory PJ, Yoon DY. Nature 1978;272:226.